Exploring the Nuclear Pasta Phase in Core-Collapse Supernova Matter

Helena Pais and Jirina R. Stone

Exploring the nuclear pasta phase in Core-Collapse Supernova Matter

Helena Pais[1] and Jirina R. Stone[1, 2, 3]

[1]*Department of Physics and Astronomy, University of Tennessee, Knoxville, TN 37996, USA*
[2]*Department of Physics, University of Oxford, Oxford OX1 3PU, United Kingdom*
[3]*Physics Division, Oak Ridge National Laboratory, Oak Ridge, TN 37831, USA*

The core-collapse supernova (CCSN) phenomenon, one of the most explosive events in the Universe, presents a challenge to theoretical astrophysics. Of the large variety of forms of matter present in CCSN, we focus on the transitional region between homogeneous (uniform) and inhomogeneous ("pasta") phases. A three-dimensional, finite temperature Skyrme-Hartree-Fock (3D-SHF) + BCS calculation yields, for the first time fully self-consistently, the critical density and temperature of both the onset of the pasta in inhomogeneous matter, consisting of neutron-rich heavy nuclei and a free neutron and electron gas, and its dissolution to a homogeneous neutron, proton and electron liquid. We also identify density regions for different pasta formations between the two limits. We employ four different forms of the Skyrme interaction, SkM*, SLy4, NRAPR and SQMC700 and find subtle variations in the low density and high density transitions into and out of the pasta phase. One new stable pasta shape has been identified, in addition to the classic ones, on the grid of densities and temperatures used in this work. Our results are critically compared to recent calculations of pasta formation in the Quantum Molecular Dynamics (QMD) approach and Thomas Fermi (TF) and Coexisting Phase (CP) approximations to Relativistic Mean Field (RMF)models.

The complex structure of nuclear matter in the density region below $\rho_s \sim 0.16$ fm^{-3} (the central density in heavy nuclei) at finite temperature ($T < 20$ MeV) critically affects many astrophysical and nuclear physics phenomena. These include the physics of neutron stars, the mechanism of core-collapse supernovae (CCSN) and the nucleosynthesis of heavy chemical elements in the Universe. Some nuclear physics properties of nuclear matter can be studied in terrestrial laboratories with new neutron-rich radioactive beams, and in relativistic heavy-ion collisions, in which similar densities and temperatures can be produced, but many aspects have to rely on theoretical models.

In this paper we concentrate on CCSN, a process which includes a large range of physical phenomena, from gravity to microscopic properties of atomic and subatomic particles. The key microscopic input into CCSN model simulations is the Equation of State (EoS), connecting the pressure of stellar matter to its energy density and temperature, which are, in turn, determined by its composition and interactions between its components. The composition of CCSN matter changes with increasing density and temperature. Initially an inhomogeneous phase exists, made up of discrete heavy nuclei immersed in a sea of single nucleons (predominantly neutrons), light nuclei (deuterons, tritons, helions, α-particles) and electrons. At higher density and temperature a homogeneous phase evolves, consisting of nucleons, strange baryons, mesons and possibly quarks.

One of the most intriguing phases of CCSN matter is the transitional region between the inhomogeneous and homogeneous phases. Initially increasing density (and a corresponding increase in neutronization driven by electron capture) drives the composition to heavier spherical or near spherical nuclei. As the density and temperature increase, further heavy quasi-nuclear structures are formed which undergo a series of changes from spherical to exotic forms: rods, slabs, cylindrical holes, and spherical holes (bubbles), termed "nuclear pasta" [1]. This process is caused primarily by the competition between surface tension and the Coulomb repulsion of closely packed heavy nuclei and occurs not only in CCSN matter (where compression was also suggested as a possible mechanism of pasta creation [2]) but also at the transitional region between the crust and core of cold neutron stars (NS). Although there are obvious similarities in these two cases, the differences in temperature (CCSN high, NS low) and isospin (CCSN low, NS high) regimes require specific treatment of each of them. This work focuses on the CCSN case, leaving the NS matter for future investigations.

The occurrence of pasta phase in CCSN and NS are two astrophysical examples of "frustrated matter". Generally, frustration occurs when a system is forced to a self-organized excited state by constraints on some of its degrees of freedom and prevented from a transition to its natural equilibrium state. The constraints are a consequence of a close competition between different interactions acting in the system. It turns out that under those circumstances a bizarre ordering is observed not only in nuclear matter, but in a variety of amorphous solids, crystals and magnetic and biological materials [3–5].

Earlier CCSN simulations used EoS which did not include the pasta phase. The most frequently used EoS were developed by Lattimer and Swesty [6], based on the compressible liquid drop model and the non-relativistic Skyrme force , and by Shen et al.,[7], who used the Thomas-Fermi (TF) approximation with a relativistic mean-field (RMF)

model. Recently published new EoS for CCSN simulations [8, 9] use the virial EoS at low density and Hartree RMF in both the inhomogeneous and uniform matter regions. Hempel et al. [10] reported calculations based on the nuclear statistical equilibrium model, which includes excluded volume effects and RMF interactions. In all the above EoS the transition to homogeneous matter is treated empirically, as the inhomogeneous (gas) and homogeneous (liquid) phases are described by different EoS. The pasta phase has not been included although, according to some estimates, it may form 10 - 20% of the core of the collapsing star [11, 12].

Other models have included the pasta phase. Sonoda et al. [12] examined the phase diagram of CCSN matter in the Quantum Molecular Dynamics (QMD) framework. They identified a sequence of spherical, cylindrical and slab-like nuclei, followed by cylindrical and spherical holes as canonical pasta phases and studied their development as a function of density and temperature. Avancini et al. [13–16] studied the pasta phase at finite temperatures within a TF approach and the coexisting phase (CP) method both at fixed neutron/proton ratios and in β-equilibrium matter. They use RMF models, both with constant and density-dependent couplings, to describe this frustrated system and determine the density regions for appearance of the classical pasta phases as a function of temperature for different variants of their models. Watanabe et al. [17] explored pasta formation in CCSN matter in the QMD approach and demonstrated that a lattice of rodlike nuclei can be formed from a bcc lattice by compression. They also found that, in the transition process, the system undergoes a zigzag configuration of elongated nuclei, which are formed by a fusion of two originally spherical nuclei.

The main interest in the pasta phase in CCSN is that the neutrino opacity, which plays the main role in the development of a shock wave during the supernova collapse, is affected by its presence [11]. Horowitz et al. [18, 19] studied these effects using the QMD technique but did not get a conclusive answer because they did not reproduce all the classical pasta shapes in their model. Sonoda et al. [11] showed how pasta phases affect the neutrino transport cross section via weak neutral current using several nuclear models. They calculated neutrino opacity of the phases with rod-like and slab-like nuclei taking into account finite temperature effects, using the QMD approach. They found that pasta phases affect the energy-dependent cross sections for coherent scattering of neutrinos in collapsing cores.

All these existing treatments of the approach to the homogeneous phase have involved considerable simplifications. The QMD approach is a semiclassical microscopic treatment, in which a large number of nucleons are dynamically evolved in a large cubic box with periodic boundary conditions without assumptions on the quasi-nuclear structure produced. It offers a computationally manageable model, but important details of nuclear structure physics are cumbersome to include in such calculations. In order to accelerate the calculations (in some cases using special purpose computational hardware) the effective nucleon-nucleon interaction is rather schematic and, among other simplifications, important shell effects are missing. The TF and CP methods represent simplifications which allow faster calculations, but may miss some important physics.

This work offers a fundamentally improved, fully self-consistent, treatment across the phase development with far fewer simplifications. We have used a non-relativistic, Skyrme-Hartree-Fock model throughout in three dimensions (3D-SHF) at finite temperature. Four different Skyrme interactions have been employed. SkM* and SLy4 (in order to compare the present results with those obtained in our previous work [20]) and NRAPR and SQMC700 (representative of the Skyrme parameter sets, found to be consistent with a wide range of constraints on nuclear matter properties [21]) were chosen. The model was first used by Newton and Stone [20, 22] and we refer the reader to these references for a detailed description of all relevant technical matters. In the calculation, it is assumed that, at a given density and temperature, matter is arranged in a periodic structure throughout a sufficiently large region of space for a unit cell to be identified. Only a single unit cell needs to be calculated to obtain the bulk properties of the matter. Cubic cells with periodic boundary conditions are used. In addition, reflection symmetry across the three Cartesian axes is assumed. This assumption allows getting the 3D-SHF solutions only in one octant of the unit cell which results in a considerable reduction of computer time. The periodic boundary conditions, the choice of the form of the initial wave function in the solution of the Hartree-Fock equations, the effect of the cell size and both the physical and spurious shell effects are discussed in detail in [20, 22]. BCS pairing correlation was included in the calculation although it is less important at finite than at zero temperature. The pairing strength decreases with increasing temperature and the single-particle occupation probabilities are mainly given by the Fermi-Dirac distribution.

The absolute minimum of the free energy of a cell containing A nucleons in the pasta phase is known not to be particularly pronounced and multiple local minima are expected. In order to systematically survey the "shape space" of all nuclear configurations of interest, the quadrupole moment of the neutron density distributions has been parameterized, and those parameters constrained (the proton distribution is found to follow that of the neutrons). In all cases studied in this work, we set the proton fraction equal to 0.3, a likely value for CCSN matter. The minimum of the free energy in a cell at a given particle number density, temperature and proton fraction is sought as a function of three free parameters: the number of particles in the cell (determining the cell size) and β, γ, the parameters of the quadrupole moment of the neutron distribution. Each minimization takes approximately 12 hours of CPU time

on a single core of the Cray XT5/XK6 machine and is performed in a trivially parallel mode, typically using 45,000 processors.

We present here a complete calculation for $T = 2$ MeV and the particle number density range 0.02 - 0.12 fm^{-3}. We observed the onset of the pasta phase and its dissolution to uniform matter. All classical pasta formations, starting from spherical droplets through rods, slabs, tubes (cylindrical holes) and bubbles (spherical holes) were observed fully self-consistently for all Skyrme force models. The shapes are illustrated in Fig. 1 for the SMC700 Skyrme force as an example at threshold densities for each shape. We show the 3D image in the top row and the yx, xz and yz projections in the 2nd, 3rd and 4th rows, respectively. In the tube and bubble regions we found the cylindrical (spherical) holes appearing exactly in the edges (corners) of the unit cell and not in the center as expected in the bcc or fcc symmetries, which are in principle allowed in a cubic box. The reason for this effect is likely to be that in our model we calculate the density distribution only in one octant of the cell and assemble the whole cell using reflection symmetry. This procedure reduces the higher order bcc and fcc symmetries to a simple cubic symmetry. The use of reflection symmetry makes the 3D-SHF model manageable. Removal of that symmetry would increase the demand on computational time by a factor of 8 which is not realistic at this time.

In addition, we determined the transition densities between individual phases as shown in Fig. 2. For comparison, we give the results for QMD model 2 (QMD2) [12] in the figure caption. Our transitions appear to be rather sharp and occur within 0.002 fm^{-3} or less density change without any obvious intermediate regions. However, we observe a stable shape, occurring for all four Skyrme models, between the rods and slabs (a cross-rod) in the low density region between 0.03 - 0.05 fm^{-3}. This formation may be akin to the "spongelike" intermediate phase reported in [12] and denoted (C,S). We, however, do not have an equivalent to their (S,CH) structure between slabs and cylindrical holes. Comparison with the most recent work of Avancini et al. [16] who used TF and CP approximations to RMF with NL3 and TW Lagrangians reveals more similarities in the phase diagrams, although the cross-rod formation has not been reported in [16]. Unfortunately detailed comparison of threshold densities for individual pasta phases cannot be made as we do not have results at temperatures used in [16].

In Table I we compare our results for the temperature dependence on the onset density of homogeneous matter with those obtained by Sonoda et al. [12] and Avancini et al. [16]. Our model and that of Avancini et al. [16] predict a slower decrease of the threshold density with temperature in comparison with [12] who do not observe pasta phase at all at $T = 10$ MeV. This is illustrated in Fig. 3 where the average for the four Skyrme interactions, the TF and CP models for NL3 and TW interaction and the QMD2 model results are plotted against temperature.

It has been suggested on the basis of QMD models [12, 17] that the slope $L(\rho_0) = 3\rho_0 \frac{\partial E_{sym}(\rho)}{\partial \rho}|_{\rho=\rho_0}$ of the symmetry energy E_{sym}, calculated at nuclear saturation density ρ_0, is inversely related to the critical temperature T_c at which pasta disappears, i.e. the higher value of L, the lower would be the critical temperature. However, as seen in Table II, the NL3 model has significantly higher value of L than the QMD2 and yet, both it, and the present calculation, which have the lowest L values, predict T_c well above that of QMC2. Thus the proposed relation between L and T_c does not appear to hold universally.

In conclusion, we have identified, fully self-consistently, the onset of the pasta phase in inhomogeneous CCSN matter consisting of neutron-rich heavy nuclei and a free neutron and electron gas and its dissolution to homogeneous neutron, proton and electron liquid. The density range of the pasta phase is temperature dependent; it decreases with increasing temperature. On the currently used density/temperature grid, all accepted shapes have been identified with one new cross-rod shape. The slab phase is found over the widest density range. Although this is true for all four interactions used, the particular widths of the various pasta phases show interesting variation. Consistent with the Avancini et al. result, we find that, for temperatures higher than 2 MeV, the transition density from the pasta phase to homogeneous matter decreases far more slowly with increasing temperature than the QMD result. The results of this work, extended to relevant temperatures and proton/neutron ratios, will be used to construct four EoS for supernova simulation models, augmented by 1D calculation at densities below and above the pasta region. Neutron and proton density distributions in the unit cell, obtained in this work, will be employed in the modeling of neutrino transport through the pasta formations. This will be the first time a continuous particle density distribution rather than individual particles will be used in such calculation.
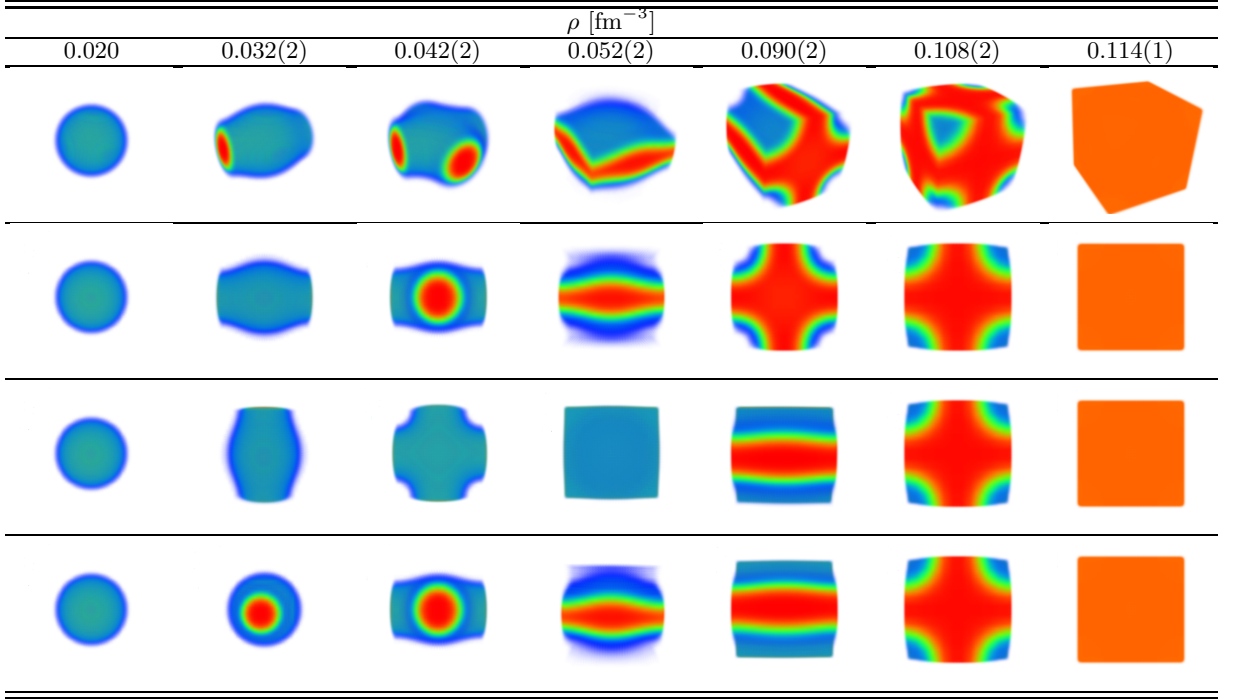
FIG. 1: (Color online) First row: Pasta phases calculated using the SQMC700 Skyrme interaction, $T = 2$ MeV and $y_{\mathrm{p}} = 0.3$. Rows 2, 3, 4: 2D projection of the pasta phases on the (y,x), (x,z) and (y,z) planes, respectively. The neutron density distribution is shown at the density corresponding to the onset of each phase, known with the uncertainty given in brackets. Blue (red) color indicates the bottom (top) of the density scale: 0.001 (dark blue) - 0.02475 (light blue) - 0.0485 (green) - 0.07225 (light orange) - 0.095 (red) fm^{-3}. The pasta formation shown here appears for all the Skyrme models, but the threshold density changes somewhat, see Fig. 2.

[1] D. G. Ravenhall, C. J. Pethick, and J. R. Wilson, Phys. Rev. Lett. **50**, 2066 (1983).
[2] G. Watanabe and T. Maruyama, arXiv:1109.3511v2 [nucl-th] (2011).
[3] G. Watanabe and H. Sonoda, *Soft Condensed Matter* (Nova Science Publishers Inc, New York, 2007).
[4] R. Moessner and A. P. Ramirez, Phys. Today **59(2)**, 24 (2006).
[5] Y. Han, Y. Shokef, A. M. Alsayed, P. Yunker, T. C. Lubensky, and A. G. Yodh, Nature **456**, 898 (2008).
[6] J. M. Lattimer and F. D. Swesty, Nucl. Phys. A **535**, 331 (1991).
[7] H. Shen, H. Toki, K. Oyamatsu, and K. Sumiyoshi, Nucl. Phys. A **637**, 435 (1998).
[8] G. Shen, C. J. Horowitz, and E. O'Connor, Phys. Rev. C **83**, 065808 (2011).
[9] G. Shen, C. J. Horowitz, and S. Teige, Phys. Rev. C **83**, 035802 (2011).
[10] M. Hempel, T. Fischer, J. Schaffner-Bielich, and M. Liebendörfer, Astrophys. J. **748**, 70 (2012).
[11] H. Sonoda, G. Watanabe, K. Sato, T. Takiwaki, K. Yasuoka, and T. Ebisuzaki, Phys. Rev. C **75**, 042801(R) (2007).
[12] H. Sonoda, G. Watanabe, K. Sato, K. Yasuoka, and T. Ebisuzaki, Phys. Rev. C **77**, 035806 (2008).
[13] S. S. Avancini, D. P. Menezes, M. D. Alloy, J. R. Marinelli, M. M. W. Moraes, and C. Providência, Phys. Rev. C **78**, 015802 (2008).
[14] S. S. Avancini, L. Brito, J. R. Marinelli, D. P. Menezes, M. M. W. de Moraes, C. Providência, and A. M. Santos, Phys. Rev. C **79**, 035804 (2009).
[15] S. S. Avancini, S. Chiacchiera, D. P. Menezes, and C. Providência, Phys. Rev. C **82**, 055807 (2010).
[16] S. S. Avancini, S. Chiacchiera, D. P. Menezes, and C. Providência, Phys. Rev. C **85**, 059904(E) (2012).
[17] G. Watanabe, H. Sonoda, T. Maruyama, K. Sato, K. Yasuoka, and T. Ebisuzaki, Phys. Rev. Lett. **103**, 121101 (2009).
[18] C. J. Horowitz, M. A. Pérez-García, and J. Piekarewicz, Phys. Rev. C **69**, 045804 (2004).
[19] C. J. Horowitz, M. A. Pérez-García, J. Carriere, D. K. Berry, and J. Piekarewicz, Phys. Rev. C **70**, 065806 (2004).
[20] W. G. Newton and J. R. Stone, Phys. Rev. C **79**, 055801 (2009).
[21] M. Dutra, O. Lourenço, J. S. Sá Martins, A. Delfino, J. R. Stone, and P. D. Stevenson, Phys. Rev. C **85**, 035201 (2012).
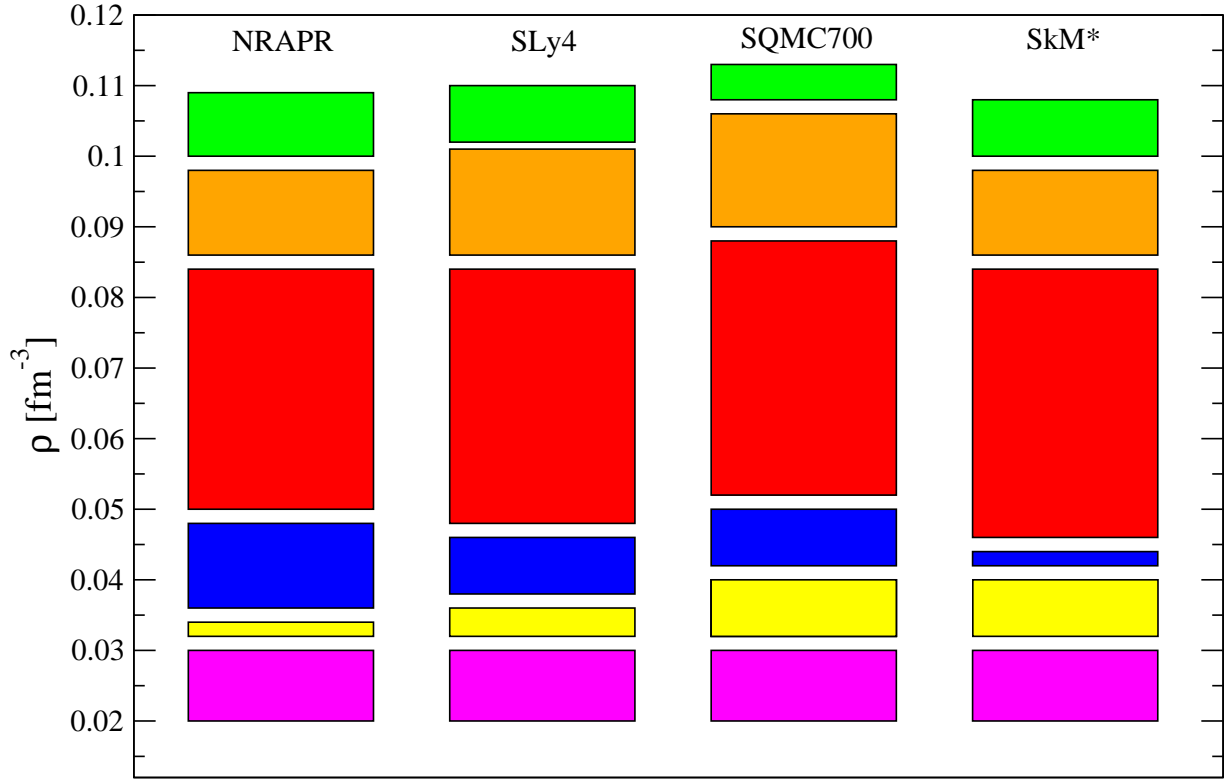[22] W. G. Newton, Ph.D. thesis, Oxford University (2008), URL http://www.tamu-commerce.edu/home/physics/newton/thesis.pdf.

FIG. 2: (Color online) Comparison of phase diagrams at $T = 2$ MeV and $y_{\mathrm{p}} = 0.3$ as calculated for the four Skyrme interactions used in the 3D-SHF model. The sequence of phases from bottom to top is spherical droplets (magenta) - no pasta, rods (yellow), cross-rods (blue), slabs (red), cylindrical holes (tubes) (orange) and spherical holes (bubbles) (green). The white gaps between colored boxes represent transition regions in which calculation is not available. The onset densities of each phase can be compared with results of Sonoda et al. [12], who found the following regions of densities (all in fm^{-3} rounded to 3 decimal places): 0.017 - 0.029 (spherical droplets), 0.034 (rods), 0.059 - 0.063 (slabs), 0.080 - 0.084 (cylindrical holes) and 0.088 - 0.109 (spherical holes).

Model T [MeV]	NRAPR	SQMC700	SkM*	SLy4	QMD2 ρ[fm^{-3}]	NL3(TF)	NL3(CP)	TW(TF)	TW(CP)
0	0.108	0.112	0.107	0.109	0.118-0.122	0.099	0.097	0.109	0.100
1					>0.118				
2	0.110	0.114	0.109	0.111	0.109-0.113				
3					0.101-0.105				
4	0.108	0.113	0.107	0.110	0.092-0.097				
5					0.084-0.088	0.092	0.091	0.103	0.094
6	0.100	0.105	0.100	0.102	0.080-0.084				
7					0.063-0.067	0.084	0.084	0.096	0.087
8	0.091	0.099	0.089	0.094	0.050-0.055	0.078	0.079	0.091	0.082
9					0.034-0.038				
10	0.075	0.079	0.074	0.077					

TABLE I: Total particle number onset densities of homogeneous matter for the interactions and temperatures studied. Results of a QMD calculation (model 2) [12] (only a range can be given in this case) and of TF and CP approximations to RMF with NL3 and TW Lagrangians [16] are added for comparison. For more discussion see text.
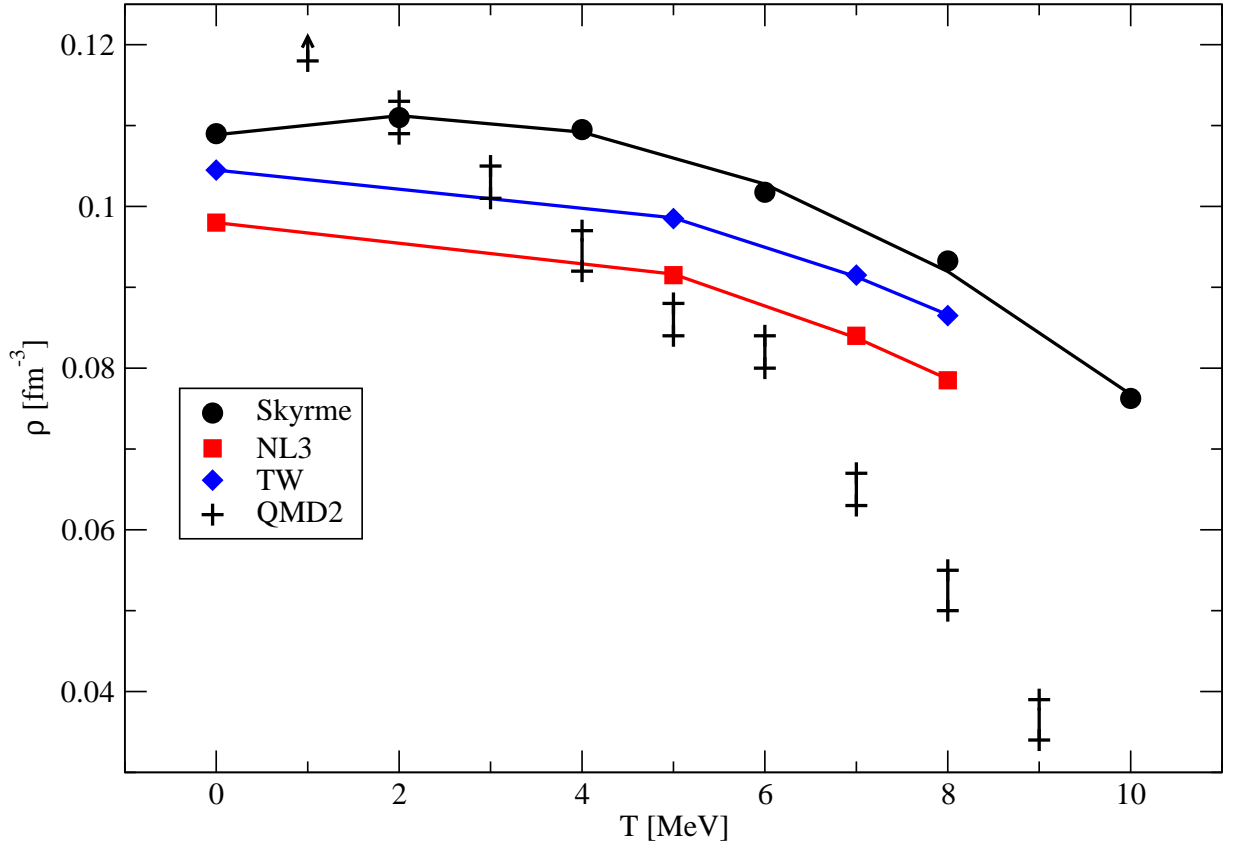
FIG. 3: (Color online) Temperature dependence on the onset density of homogeneous matter, as predicted by the Skyrme, RMF (NL3, TW) and QMD2 models. Values for QMD2 model are given as a range; the arrow shows that the entry is a lower limit. The lines are added to guide the eye. For more details see text.

Model	ρ_0	B/A	K	E_{sym}	L
NRAPR	0.16	-15.85	226	33	60
SQMC700	0.17	-15.49	222	33	59
SkM*	0.16	-15.77	217	30	46
SLy4	0.16	-15.97	230	32	46
QMD2	0.17	-16	280	33	80
NL3	0.15	-16.3	272	37	118
TW	0.15	-16.3	240	33	55

TABLE II: Symmetric nuclear matter properties at saturation density ρ_0 (energy per particle B/A, incompressibility K, symmetry energy E_{sym} and symmetry energy slope L) for the models shown in Tab. I. All the quantities are in MeV, except for ρ_0, given in fm^{-3}.